Key Points:
- Channel deepening increased the salinity intrusion by about 30%, but the response to river discharge of $\sim Q_r^{-1/3}$ remained similar
- Estuarine circulation has not changed, as depth increases were compensated by a reduction in the along-estuary salinity gradient
- Stratification has increased, particularly during neap tides, which is opposite the expectation from equilibrium scaling

Response to Channel Deepening of the Salinity Intrusion, Estuarine Circulation, and Stratification in an Urbanized Estuary

David K. Ralston[1] ID **and W. Rockwell Geyer[1]** ID

[1]Applied Ocean Physics and Engineering Department, Woods Hole Oceanographic Institution, Woods Hole, MA, USA

Abstract Modifications for navigation since the late 1800s have increased channel depth (H) in the lower Hudson River estuary by 10–30%, and at the mouth the depth has more than doubled. Observations along the lower estuary show that both salinity and stratification have increased over the past century. Model results comparing predredging bathymetry from the 1860s with modern conditions indicate an increase in the salinity intrusion of about 30%, which is roughly consistent with the $H^{5/3}$ scaling expected from theory for salt flux dominated by steady exchange. While modifications including a recent deepening project have been concentrated near the mouth, the changes increase salinity and threaten drinking water supplies more than 100 km landward. The deepening has not changed the responses to river discharge (Q_r) of the salinity intrusion ($\sim Q_r^{-1/3}$) or mean stratification ($Q_r^{2/3}$). Surprisingly, the increase in salinity intrusion with channel deepening results in almost no change in the estuarine circulation. This contrasts sharply with local scaling based on local dynamics of an H^2 dependence, but it is consistent with a steady state salt balance that allows scaling of the estuarine circulation based on external forcing factors and is independent of depth. In contrast, the observed and modeled increases in stratification are opposite of expectations from the steady state balance, which could be due to reduction in mixing with loss of shallow subtidal regions. Overall, the mean shift in estuarine parameter space due to channel deepening has been modest compared with the monthly-to-seasonal variability due to tides and river discharge.

1. Background

Around the world, major cities and towns have developed near estuaries to take advantage of benefits for transportation and supply of food and water. For centuries humans have modified the physical conditions in estuaries to enhance those benefits, including by constructing navigational channels, filling shallow regions for development, and regulating river discharges. Modifications to estuarine bathymetry can alter hydrodynamics and affect basic processes like tidal propagation, exchange with the coastal ocean, and the salinity distribution, which in turn can affect sediment transport, residence time, and biogeochemical processes. With sufficiently long term observational records, effects of anthropogenic modifications can be identified as trends or discrete changes in estuarine conditions, but these changes can be difficult to discern amidst the natural variability due to the tides, river discharge, or storm events.

Time series of water surface elevation extending back a century or more have shown that deepening of estuarine channels for navigation is often associated with an increase in tidal amplitude. Examples include the Thames (Amin, 1983), Gironde (Jalón-Rojas et al., 2018), Elbe, Ems, and Loire (Winterwerp et al., 2013) in Europe and the Delaware (DiLorenzo et al., 1993), Columbia (Jay et al., 2011), Cape Fear (Familkhalili & Talke, 2016), and Hudson River (Ralston et al., 2019) estuaries in the United States. Increased channel depth, channel straightening, and removal of bedforms by dredging all reduce frictional damping of the tide, leading to increased tidal range in the estuary. Similarly, storm surge propagation in the estuary can increase with reductions in friction due to dredging (Familkhalili & Talke, 2016; Ralston et al., 2019). In contrast, deepening and straightening of channels and the reduction in friction can have the opposite effect on water levels during major river discharge events, reducing the overall risk of flooding in parts of an estuary (Ralston et al., 2019).

Long-term measurements of salinity and currents are less commonly available than water level records. Observations from San Francisco Bay found that the seasonal variability in the salinity intrusion has decreased over the historical record and that these changes were predominantly due to flow regulation by major reservoirs constructed since the 1960s rather than changes in estuarine geometry (Hutton et al.,

2015). In the Yangtze River, landward increases in the salinity intrusion that threaten drinking water for Shanghai have been attributed to dredging of a navigational channel, but without observations to directly quantify the connection (Zhang et al., 2011). Observations from Kill van Kull, a strait in New York Harbor, before and after a recent deepening project found a 15% increase in depth corresponded with a doubling of the estuarine circulation (Chant et al., 2018). The effects on salinity were less pronounced, with slight increases in the bottom salinity and along-estuary salinity gradient after deepening. As detailed below, that study also raised important questions about how the expected response of the estuarine circulation, stratification, and salinity distribution to deepening based on theory depends greatly on the assumptions underlying the theoretical framework.

1.1. Theoretical Background

The steady state theory based on a local dynamical balance suggests that both estuarine circulation and stratification increase nonlinearly with water depth (Hansen & Rattray, 1965; MacCready & Geyer, 2010). Based on a balance between the along-estuary pressure gradient and vertical stress divergence, the estuarine circulation (u_e) is

$$u_e = \frac{1}{48} \frac{\beta g \frac{\partial s}{\partial x} H^3}{K_M} \tag{1}$$

where H is the water depth, $\partial s / \partial x$ is the along-estuary salinity gradient, K_M is the eddy viscosity, β is the coefficient of saline contraction, and g is gravitational acceleration. Assuming that $K_M \sim U_t H$, where U_t is the tidal velocity, this suggests that the estuarine circulation scales with H^2. Similarly, using a local salt conservation balance between creation of stratification by the estuarine circulation and destruction by tidal mixing, the mean stratification scales as

$$\Delta s \sim u_e \frac{H^2}{K_S} \frac{\partial s}{\partial x} \tag{2}$$

where K_S is the eddy diffusivity. If $K_S \sim K_M / Sc \sim U_t H / Sc$, where Sc is a Schmidt number, then the stratification scales as H^3.

Together, the estuarine circulation and mean stratification produce a landward salt transport that in many estuaries is the dominant means of exchange with the coastal ocean (MacCready & Geyer, 2010). If the import of salt by the estuarine circulation is balanced by the export of salt by the mean advection due to river discharge (Q_r), then $\partial s / \partial x$ can be shown to depend on $Q_r^{-1/3} H^{-2}$ (Chant et al., 2018; MacCready, 1999; MacCready & Geyer, 2010). Alternatively, assuming salinity decreases linearly from S_0 at the seaward boundary, the length of the salinity intrusion (L_x) varies as

$$L_x \sim \frac{(g \beta S_0)^{2/3} A^{1/3} H^{5/3}}{Q_r^{1/3} U_t} \tag{3}$$

where A is the cross-sectional area (Monismith et al., 2002; Ralston et al., 2008). Using this linear approximation of $\partial s / \partial x \approx S_0 / L_x$, the estuarine circulation can be rewritten as

$$u_e \approx \frac{2}{3} \left(\frac{\beta g S_0 Q_r}{W} \right)^{1/3} \tag{4}$$

where W is the estuary width, equal to the cross-sectional area divided by the depth (A/H; Chant et al., 2018; MacCready & Geyer, 2010). This scaling indicates that if the salinity intrusion is allowed to expand landward as a result of the increase in steady salt flux with increased depth, then at steady state the increase in water depth should have no effect on the estuarine circulation. This is in sharp contrast to the result from the local balance (equation (1)) where the estuarine circulation increases with H^2 (equation (1)).

As with the estuarine circulation, assuming a steady state balance, the expression for the mean stratification can be rewritten as (Chant et al., 2018; MacCready & Geyer, 2010)

$$\frac{\Delta s}{S_0} \approx \frac{7}{H} \left(\frac{Q_r}{W(\beta g S_0)^{1/2}} \right)^{2/3} \tag{5}$$

(Chant et al., 2018; MacCready & Geyer, 2010) This suggests that stratification decreases as H^{-1} as the channel is deepened, again a very different result to the response expected from the local dynamics of an increase with H^3 (equation (2)).
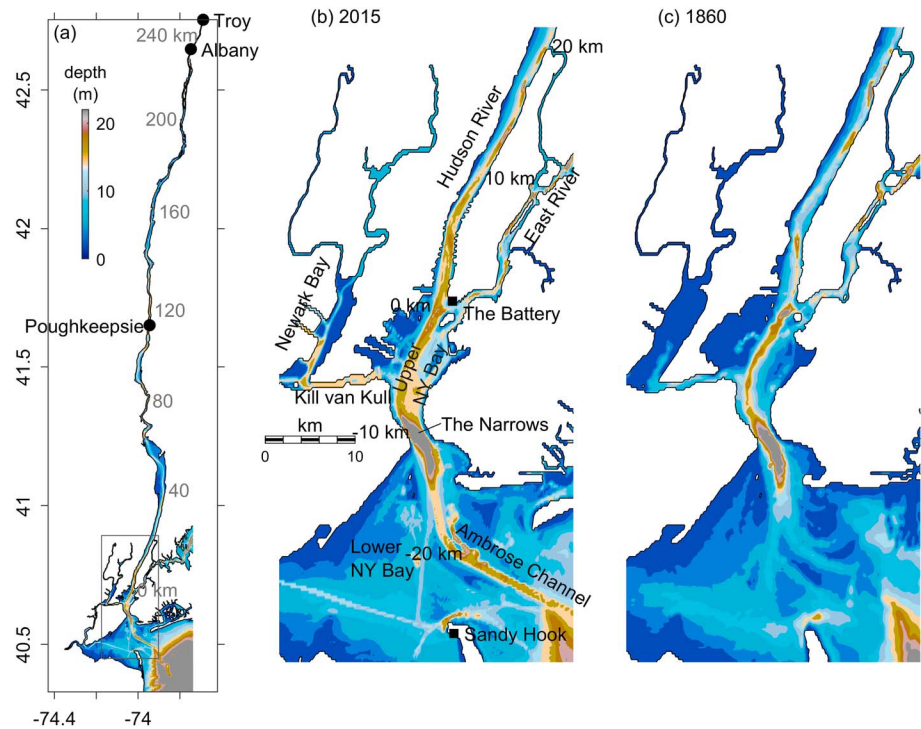
Resolving these discrepancies using observational data is challenging, given the paucity of long-term records of estuarine circulation or salinity. Observations from Kill van Kull showed a doubling of the estuarine circulation after deepening (and a modest decrease in tidal velocity) that was largely consistent with the H^2 dependence from the local balance, but this was interpreted as being due to constraints on the expansion of the salinity intrusion due to basin geometry and consequently an increase in $\partial S / \partial x$ (Chant et al., 2018). A modeling study of Tampa Bay comparing bathymetry cases representing the late 1800s and modern conditions found that increases in estuarine circulation were generally consistent with the local scaling from Hansen and Rattray (1965), but with the response varied between no change and a factor of 4 increase (Meyers et al., 2014). Another modeling study of potential deepening of the navigational channel in Tampa Bay from 12 to 18 m predicted a doubling of the estuarine circulation and a 2- to 4-practical salinity unit (psu) increase of salinity in the upper parts of the estuary (Zhu et al., 2015). A modeling study of San Francisco found that the estuarine circulation and steady salt flux increased in a modern simulation compared with predevelopment conditions due to channel deepening but that the salinity intrusion also expanded landward (Andrews et al., 2017). The modeling and limited observations so far do not provide clear guidance on the dynamical response of an estuary to past or future channel modifications.

1.2. Hudson River Estuary

To assess the response of estuarine circulation and salinity to channel deepening, we combine long-term observations and high-resolution modeling in the Hudson River estuary. The Hudson is a partially mixed estuary on the U.S. East Coast with a mean tidal range of about 1.5 m at its mouth and a region of tidal influence that extends about 250 km landward. The mean river discharge at the tidal limit from the Upper Hudson and Mohawk Rivers is about 400 m³/s, and smaller tributaries along the estuary increase the flow by 30–60% (Lerczak et al., 2006; Wall et al., 2008). The length of the salinity intrusion varies seasonally between about 60 km from the mouth during high-discharge periods and 140 km during low flow (Abood, 1974; Bowen & Geyer, 2003; Ralston et al., 2008).

New York City developed around the natural harbor at the mouth of the Hudson River. Physical changes to the estuary began with some of the first European settlers in the early 1600s (Ralston et al., 2019), as infilling of shallow regions narrowed and deepened tidal channels of the Upper New York Bay and lower Hudson River (Klingbeil & Sommerfield, 2005). Active dredging began in the late 1800s through the hazardous shoals at the mouth of the Lower Bay. Prior to dredging, the shoals were about 22 ft (6.7 m) deep, but the construction of Ambrose Channel increased that to 40 ft (12 m) by 1913. Navigational channels and anchorages were dredged to facilitate traffic to port facilities on the Upper Bay and lower Hudson, but by the 1930s much of the shipping and deepest navigational channels shifted to Newark Bay, which is connected to the Upper Bay through Kill van Kull (Figure 1). Channel deepening projects have incrementally increased navigational channel depth over the past century, the most recent being the Harbor Deepening project completed in 2016 that increased the controlling depth through the Upper Bay to 50 ft (14 m).

Investigation of estuarine processes in the Hudson extends back to around the same time as the first major dredging operations. Observations in 1858 in the Narrows between the Upper and Lower Bays found an "underrun" current carrying salt water landward and determined it was associated with the along-estuary density gradient, noting that the shallow bar at the mouth impeded "communication with the sea" (Mitchell, 1887). The same study reported that the Highlands, a deep, narrow section about 70 km landward from the Battery, had been "invaded by the sea" with salty near-bottom water during low-discharge conditions. More recent studies have demonstrated that the along-estuary salinity distribution in the Hudson is controlled primarily by a balance between the landward salt transport by the estuarine circulation (or "underrun") and the seaward transport by the river flow (Lerczak et al., 2006; Ralston et al., 2008). Observations under low to moderate discharge found that variability in the equilibrium salinity intrusion

Figure 1. Hudson bathymetry. (a) The model domain, from New York Bight to the tidal limit of the Hudson River; (b) the modern (2015) bathymetry in New York Harbor and the Lower Hudson Estuary; and (c) the predredging (1860) bathymetry in the same region.

was consistent with the estuarine circulation scaling of $Q_r^{-1/3}$ (Abood, 1974). A simple model of a time-dependent balance between the estuarine circulation and mean outflow represented observed variability in the salinity distribution at spring-neap and seasonal time scales (Ralston et al., 2008), suggesting that this conceptual framework represents well the dominant dynamics in the Hudson.
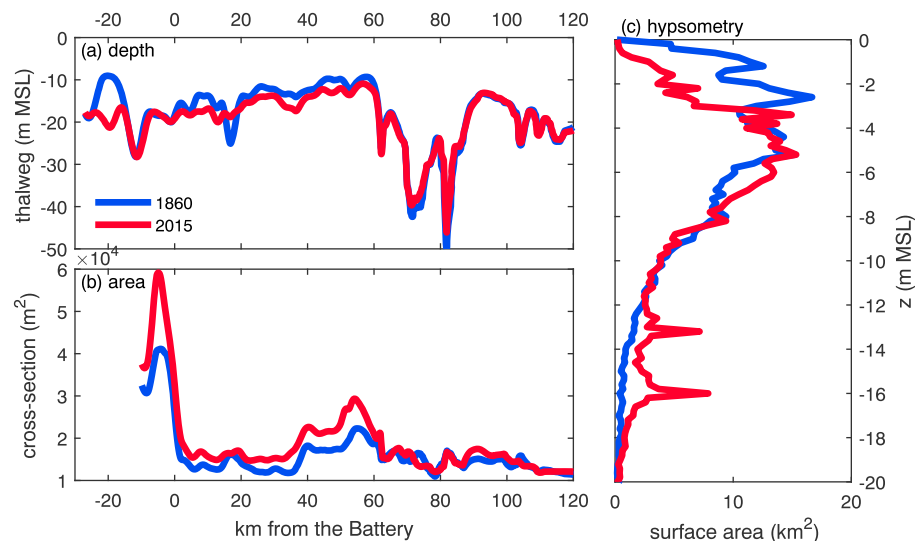
2. Methods and Data Sources

This study focuses on the response of the estuarine circulation, salinity distribution, and stratification to bathymetric changes in the Hudson, but a companion study focused on changes in the tides, storm surge, and flooding (Ralston et al., 2019). Many of the methods and data sources overlap, so we provide an overview here and refer to the previous study for additional details.

2.1. Bathymetry

Bathymetry data were collected to represent conditions in the estuary at different points in time for use in numerical model grids. The earliest available navigational charts in the region were published in the 1860s and were based on hydrographic surveys from 1856 to 1858, predating the start of major channel modifications. The charts were digitized and projected on a regular grid (Ralston et al., 2019). The modern bathymetry was based on data from New York State Department of Environmental Conservation, the National Oceanic and Atmospheric Administration (NOAA), and the U.S. Army Corps of Engineers (Ralston et al., 2019) and was projected onto the same regular grid. Bathymetric survey data were referenced to a tidal datum (mean lower lowwater (MLLW)) and converted to mean sea level (MSL) based on modern survey data (using NOAA's VDatum software) or tidal amplitudes from historical water level records and charts (Ralston et al., 2019). From the 1860s to 2015 MSL at the Battery increased by about 0.44 m (Talke et al., 2014), and the effect of this on estuary depth is incorporated in the bathymetry observations in addition to the more local changes.

Nominally, the historical and modern bathymetries represent conditions in 1860 and 2015 (Figure 1). The increases in thalweg depth over this period vary along the estuary but are greatest near the mouth at Ambrose Channel (−20 km), where depth has more than doubled, and in the lower Hudson between the

Figure 2. Along-channel bathymetry and hypsometry. (a) Thalweg depth along the estuary versus distance from the Battery for the predredging (1860) and modern (2015) conditions; (b) cross-sectional area; and (c) hypsometry in the Harbor and lower Hudson (<60 km from the Battery).

Battery (0 km) and Haverstraw Bay (60 km), where depths have increased by 10–30% (Figure 2). Note that by convention and for comparison with previous studies the distances along estuary are referenced to the Battery at the southern tip of Manhattan. The cross-sectional area of the estuary has increased in these same regions, which corresponds to a reduction in the mean outflow velocity of Q_r/A (Figure 2). The bathymetric changes reflect deepening of both the main channel and adjacent shoal regions due to lateral encroachment for development. Comparing the hypsometry of the estuary between the mouth and Haverstraw, the modern estuary has less intertidal and shallow subtidal area; more area now is greater than 6 m below MSL, including the distinct navigational channels at about 13 and 16 m (Figure 2).
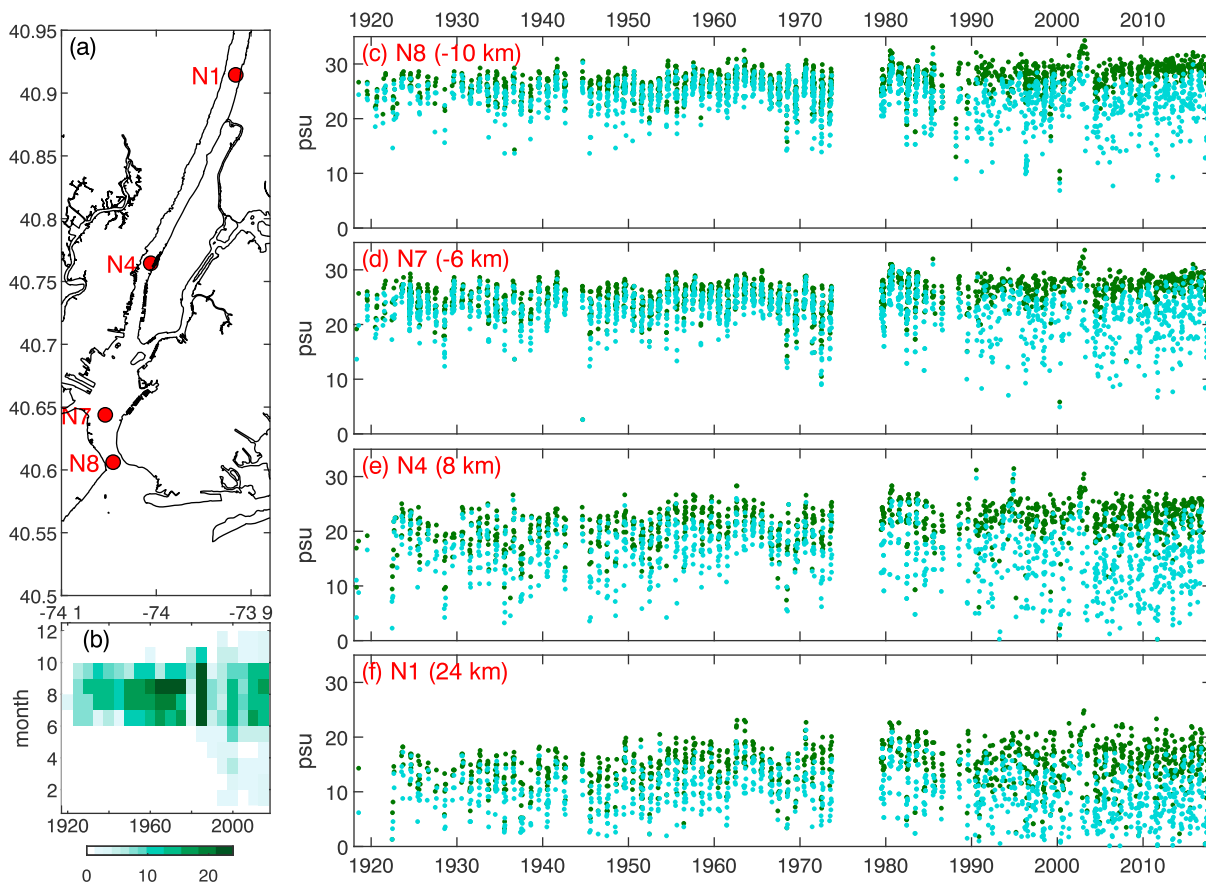
In addition to the 1860 and 2015 cases based on Ralston et al. (2019), a model bathymetry representative of conditions in 1995 was developed for simulations corresponding with observations from that year. The major bathymetric changes between 1995 and 2015 were due to the Harbor deepening project that increased the controlling depths to 50 ft (15.2 m) in New York Harbor and the surveyed depth in Ambrose Channel to 54 ft (16.5 m). In the bathymetric survey from 1995 the controlling depth in Ambrose Channel was 45 ft (13.7 m). To make the 1995 bathymetry grid, the navigational channels at the mouth and in the Harbor were decreased to the depths based on the bathymetric survey from 1995, as shown in the NOAA chart published in 2000.

2.2. Observed Salinity and Discharge

The city of New York has been collecting water samples in New York Harbor and the lower Hudson estuary since 1909 as part of a monitoring effort that began in response to public concerns about water quality (New York City Department of Environmental Protection, 2010). The New York Metropolitan Sewerage Commission initially established 12 monitoring stations around Manhattan, and that has expanded to about 40 stations around the Harbor. Historically, most of the sampling occurring during the summer months, when water quality tended to be lowest, but in recent decades sampling has occurred year-round (Figure 3). In addition to water quality metrics like dissolved oxygen and bacterial counts, measurements were made of near-surface and near-bottom salinity. Prior to 1968, the salinity data were reported in units of "percent seawater." These data have been converted to psu based on a definition of sea water as 18,000 mg/L chloride (New York Metropolitan Sewerage Commission, 1909), which corresponds with a salinity of 32.52 psu.

The U.S. Geological Survey (USGS) has measured salinity in the upper Hudson estuary at Poughkeepsie (#01372058, 112 km from the Battery) since 1992 (Figure 1), in part to monitor conditions near a
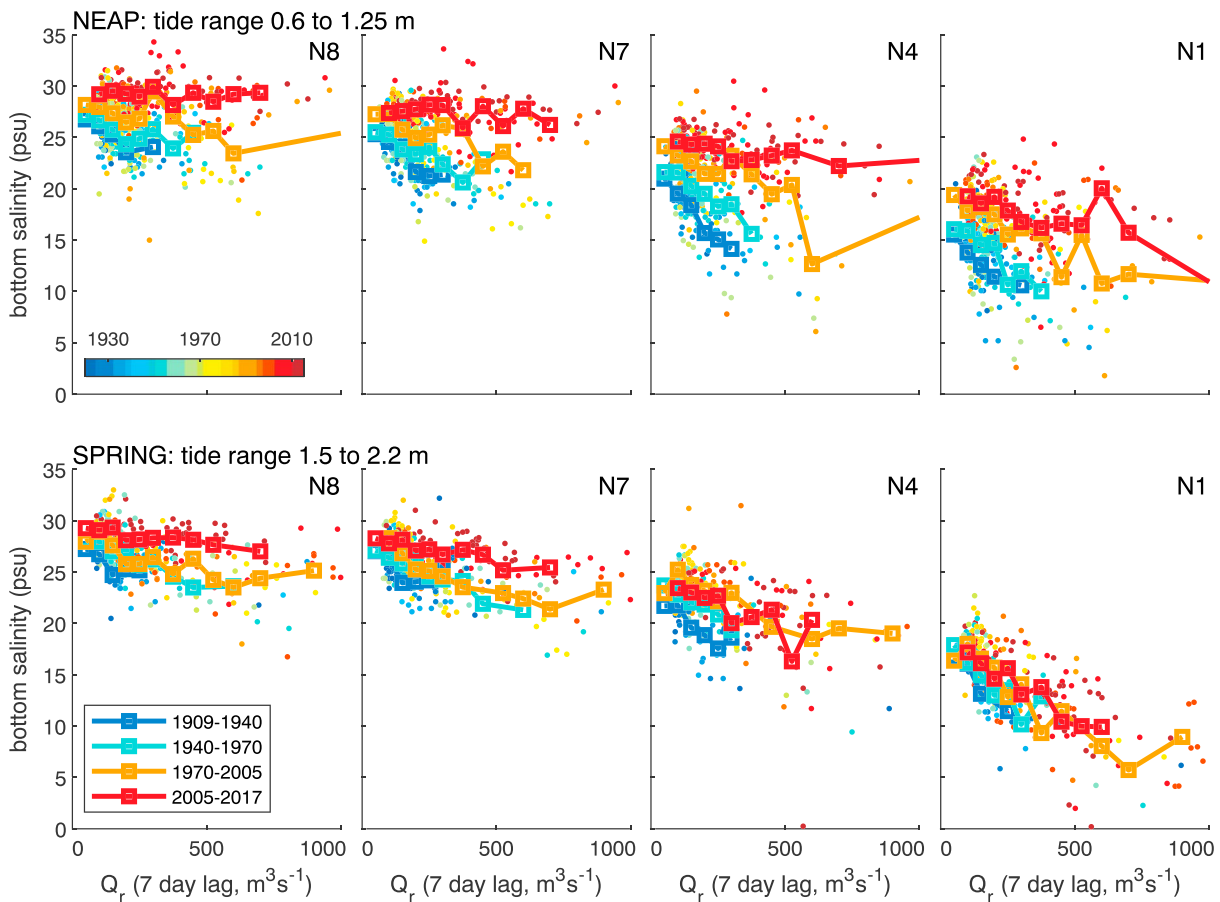
Figure 3. Salinity time series from Harbor Water Quality surveys. (a) Map with selected station locations, (b) histogram of average number of samples per month; and (c–f) bottom and surface salinity at stations, noting also along-estuary distance from the Battery.

municipal drinking water withdrawal from the Hudson. During extended periods of low river discharge, the salinity intrusion can extend to this region, potentially contaminating the water supply for the city of Poughkeepsie (Bowen & Geyer, 2003). Salinity data from this USGS station are used to inform potential management actions during droughts to release water from upstream reservoirs, increasing the total river discharge and pushing the salinity intrusion seaward of the water supply intakes. Additional data from USGS discharge monitoring stations for rivers flowing into the Hudson are used to force the model simulations, including the Mohawk at Cohoes (#01357500), the Upper Hudson at Waterford (#01335754), and Green Island (#01358000) just below the confluence of these two rivers (Ralston et al., 2019).

2.3. Circulation Model

Hydrodynamic model simulations of the Hudson and surrounding region are run using both modern and historical bathymetric configurations. The Regional Ocean Modeling System (Haidvogel et al., 2008; Warner et al., 2010) is applied to a domain extending from New York Bight to the tidal limit (Figure 1). The model grid spacing is identical for the three bathymetry cases representing 1860, 1995, and 2015. Details on the model configuration are described in Ralston et al. (2019). Simulations were run with both idealized, constant discharge forcing and realistic, time-varying forcing corresponding to periods with observational data. The idealized cases were forced with constant river discharge of 150, 300, 600, 2,000, and 5,000 m^3/s and harmonic tides with spring-neap variability. The realistic forcing scenario represents the summer of 1995. River discharge is based on measurements at the tidal limit that are increased by a factor of 1.6 to account for smaller, ungauged tributaries downstream (Lerczak et al., 2006). Water levels at the open boundaries are based on tidal harmonics using nine constituents from an ADCIRC database (Mukai et al., 2002) and observed subtidal water levels from Sandy Hook (NOAA #8531680) and Willets Point (NOAA #8516990).
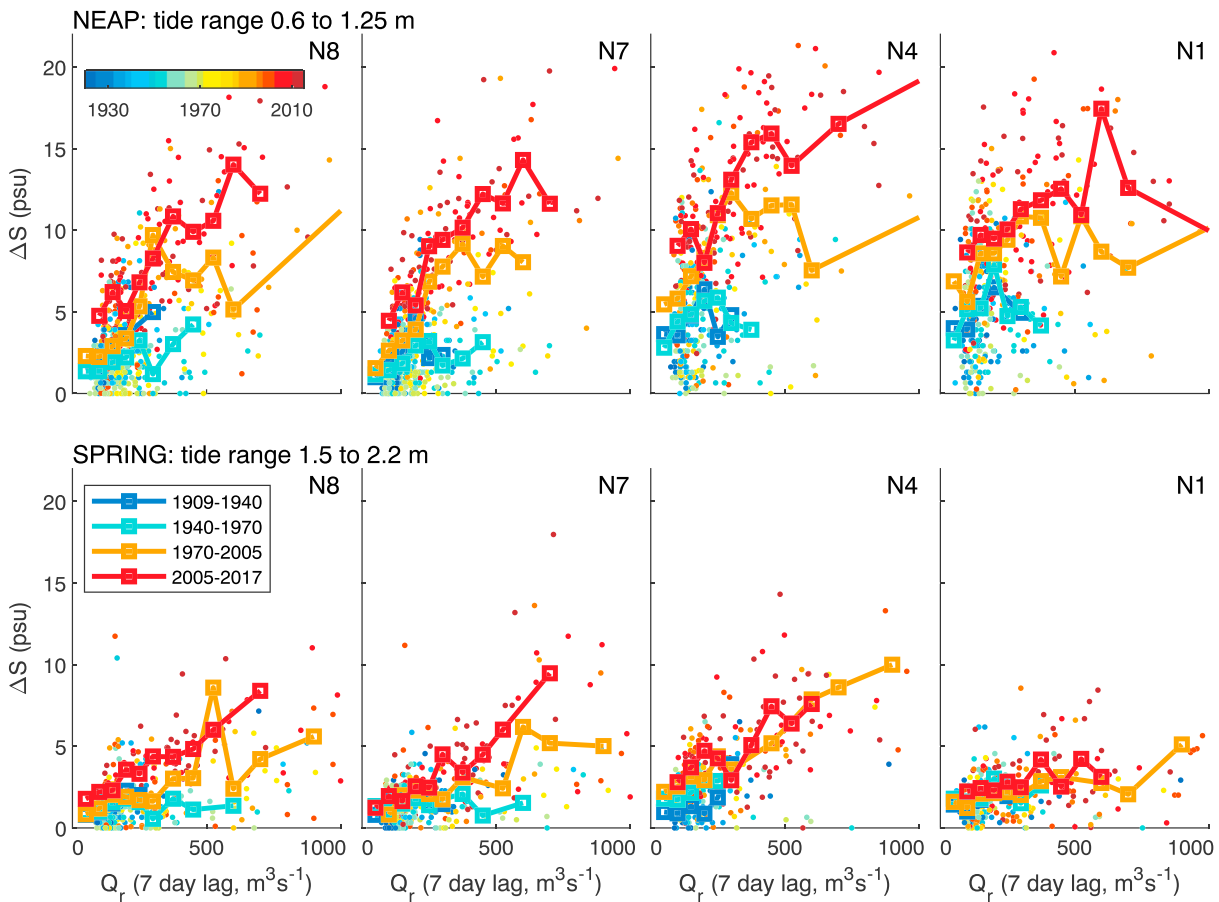
Figure 4. Bottom salinity from Harbor Water Quality survey stations N8, N7, N4, and N1 (shown in Figure 3) versus Hudson River discharge (lagged 7 days) and separated into (top) neap tide (tidal range 0.6 to 1.25 m) and (bottom) spring tide (1.5 to 2.2 m) periods.

3. Results

3.1. Observations

Surface and bottom salinity measurements have been collected at Harbor Water Quality stations since the early twentieth century, and data from four stations from the Narrows (N8, −10 km) to the lower Hudson near Spuyten Duyvil (N1, 24 km) are shown (Figure 3). The greater salinities at the more seaward stations reflect the along-estuary salinity gradient, with variability due to random sampling of tidal and discharge conditions. All of the stations show trends of increasing bottom salinity. Prior to about 1990, most of the sampling was done during the summer months (Figure 3b), and using only the data from June to September, the trends in bottom salinity range between 0.031 psu/year at N7 (−6 km, $r^2 = 0.10$) and 0.047 psu/year at N4 (8 km, $r^2 = 0.14$). The correlations of the linear regressions at all the stations are low due to the variance with the tides and river discharge, but the trends are significant ($p \ll 0.001$). Over the same period, the linear trend in daily river discharge during the summer months has had a slight increase (1.1 m³·s⁻¹·year⁻¹, $r^2 = 0.02$), which would tend to push the bottom salinity in the opposite direction of the observed change. Stratification in the summer months, or difference between bottom and surface salinity, has also increased, with trends between 0.041 psu/year at N1 ($r^2 = 0.07$) and 0.065 psu/year at N4 ($r^2 = 0.14$).

To account for some of the variability associated with the forcing conditions, the data can be plotted as functions of discharge and tidal range. Bottom salinity at the same four stations has been plotted against river discharge, separating the data into neap (tide range of 0.6 to 1.25 m) and spring (1.5 to 2.2 m) tide periods (Figure 4). The discharge is the sum of the Upper Hudson and Mohawk Rivers with a temporal lag to account for transit time and estuarine adjustment. For simplicity, the lag is fixed to 7 days based on previous studies that found that the salinity distribution correlated with discharge lagged by 5–10 days (Abood, 1974), but this

Figure 5. Stratification, or the difference between bottom and surface salinity, from Harbor Water Quality survey stations N8, N7, N4, and N1 (shown in Figure 3) versus Hudson River discharge (lagged 7 days) and separated into (top) neap tide (tidal range 0.6 to 1.25 m) and (bottom) spring tide (1.5 to 2.2 m) periods.
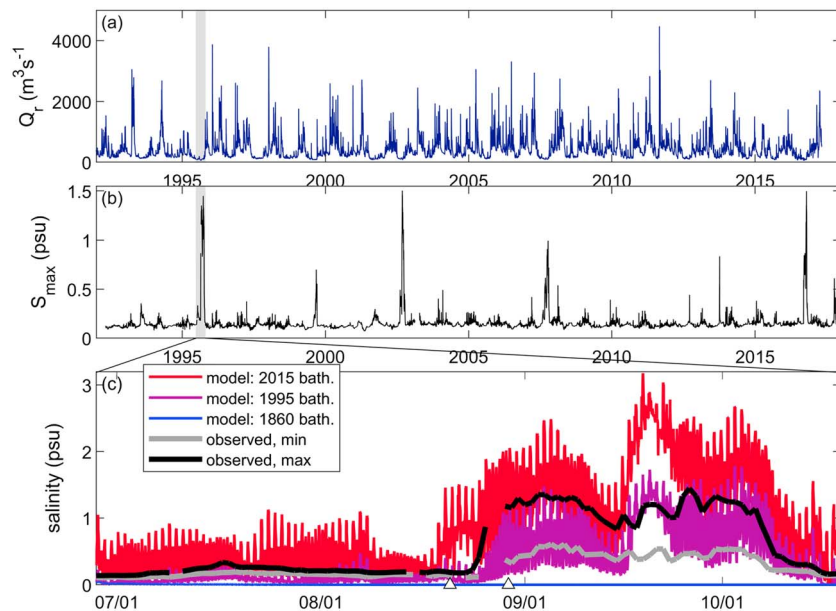
could be refined by making the lag discharge dependent. The sampling date is indicated with marker color, and data have been bin averaged into four periods with similar bathymetric conditions to highlight differences through time.

Bottom salinities for all the tidal forcing conditions show trends of decreasing salinity with increasing river discharge, consistent with a seaward shift in the salinity intrusion and decreasing salinity at a location (Figure 4). The relationships between discharge and bottom salinity also depend on sampling date, with salinity increasing during each successive period of increased channel depth, as in the time series trends. The increase in bottom salinity for a given discharge is more pronounced during neap tides than during spring tides. For example, the bin-averaged bottom salinity for Q_r of 300 m^3/s increased by 6 to 9 psu during neap tides between the pre-1940 and post-2005 periods, whereas during spring tides the increases were 2 to 3 psu.

Similarly, changes in stratification can be assessed by taking into account variability with tidal amplitude and discharge (Figure 5). In all cases, stratification increases as discharge increases, consistent with a stronger salinity gradient and enhanced by stratification due to the estuarine circulation or tidal straining (Geyer & MacCready, 2014). For a given discharge, the stratification in the more recent survey data is greater than in previous periods, and the increase in stratification over time is greater during neap tides than during spring tides. Taking Q_r of 300 m^3/s as an example again, the top-to-bottom salinity difference has increased by 5–7 psu during neaps, while the change during spring tides has been 1–2 psu. The normalized stratification, $\Delta S/S$, also has increased over the survey period, but the increase in stratification (Figure 5) is more pronounced because it also incorporates the increase in mean salinity (Figure 4).

The increase in salinity at a location with increasing channel depth indicates an increase in the landward salt flux. In the Hudson, the landward salt flux is dominated by the estuarine circulation and mean stratification
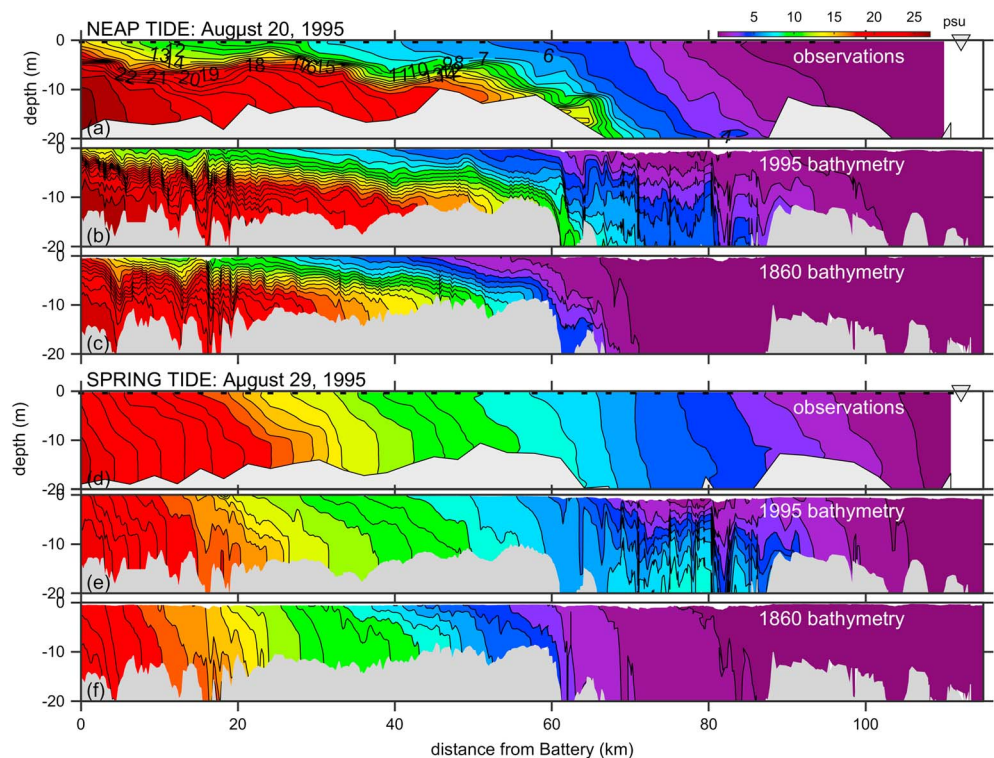
Figure 6. Salinity at Poughkeepsie (120 km from the Battery). (a) River discharge at the head of tides (Green Island); (b) daily maximum salinity at Poughkeepsie; and (c) salinity during the drought period in summer of 1995 (highlighted in upper panels), including observed daily maximum and minimum salinity along with model results using the modern (2015), circa 1995, and predredging (1860) bathymetries. Markers on the x-axis show times of along-channel surveys in Figure 7.

(Lerczak et al., 2006; Ralston et al., 2008), both of which depend on channel depth as described above. Both the estuarine circulation and mean stratification also depend inversely on tidal velocity through K_M and K_S, and the survey data are consistent with this in that the stronger mixing during spring tides reduces the salinity and stratification compared with those in neaps. During spring tides the increases in bottom salinity and stratification are relatively modest, indicating that there has not been a major shift during periods of strong mixing. However, during neap tides the positive feedback between landward salt flux and increased stratification has had more pronounced effects on increasing the salinity at a station as the channel has deepened.

3.2. Model With Realistic Forcing

The Harbor survey data present a remarkably long record of estuarine conditions over the past century, but the surveys are focused on a small part of the lower estuary and do not directly address questions about the broader estuary. Nearly continuous measurements of near-surface salinity are available starting in 1992 in the upper estuary near Poughkeepsie, about 112 km landward from the Battery. As with the Harbor Water Quality surveys, the Poughkeepsie time series started as a practical motivation to monitor water quality, in particular the salinity near a municipal drinking water intake. The salinity intrusion reaches Poughkeepsie only during periods of extended low discharge, which has occurred at roughly 3- to 6-year intervals since the observations began (Figure 6). The first example in this record of the salinity intrusion reaching Poughkeepsie was in the summer of 1995, when the daily maximum salinity was greater than 0.5 psu for about 6 weeks. This period coincided with a broader study of the estuary using moorings and shipboard surveys, which provides context for the USGS time series (Bowen & Geyer, 2003). Here we use model simulations of this period to assess the sensitivity of the salinity in the upper estuary to bathymetric changes.

Simulations were run for different bathymetric configurations, and time series were extracted at the Poughkeepsie sampling location. The simulation using the 2015 bathymetry shows an increase in salinity in mid-August and a decrease in early October, generally consistent with the timing of the salinity increase in the observations (Figure 6). However, the 2015 bathymetry case also has tidal variation in salinity of 0.5–1 psu during the several months prior to the observed increase, when the observed salinities were 0.1–0.3 psu. In contrast, the case with predredging bathymetry from 1860 has entirely fresh water at
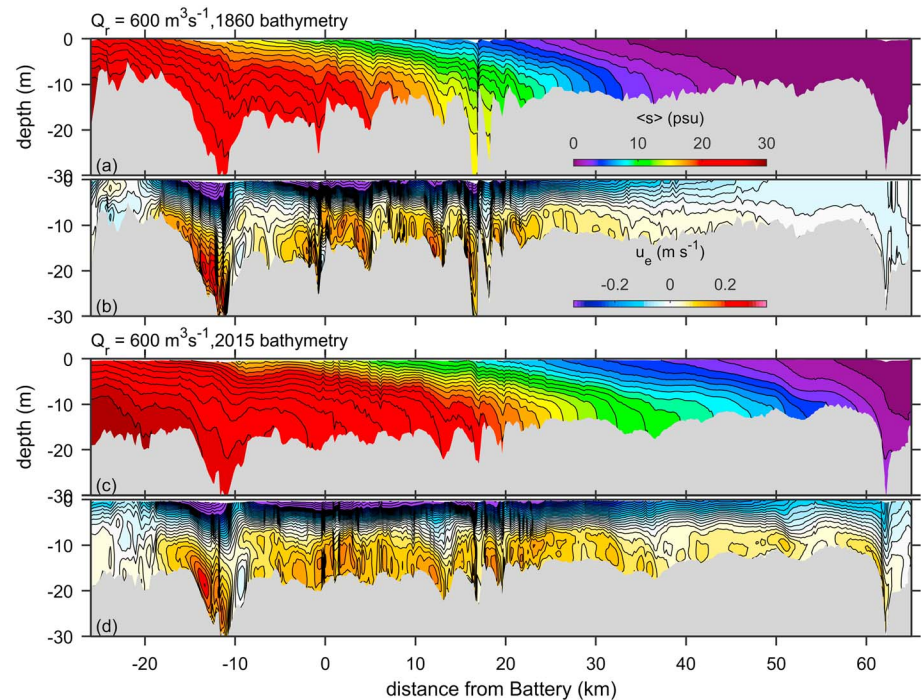
Figure 7. Along-estuary salinity profiles during low-discharge conditions in summer 1995. (a) Observation from a shipboard survey during a neap tide (20 August 1995; Bowen & Geyer, 2003), with CTD locations marked in black at the top; (b) corresponding model results using the 1995 bathymetry; and (c) model results using the 1860 bathymetry. (d) Observations during a spring tide (29 August 1995); (e) corresponding model results using the 1995 bathymetry; (f) model results using the 1860 bathymetry. The location of the U.S. Geological Survey station at Poughkeepsie (at 112 km) is marked with a triangle in (a) and (c).

Poughkeepsie throughout the drought period. The intermediate case, representing the bathymetry in 1995 based on the controlling depths at that time, results in the salinity time series at Poughkeepsie that is most consistent with the observations. The tidal variability of salinity in the 1995 model during the late summer corresponds with the observed daily maximum and minimum salinities, and the lower salinity conditions earlier in the summer are more consistent with measured values than those in the 2015 bathymetry case.

The increases in modeled salinity at Poughkeepsie with increasing channel depth are consistent with the trends from the water quality data from the Harbor and lower estuary. The depth increase since the start of dredging has changed this part of the Hudson from a freshwater tidal river to an oligohaline regime, with 0.5–1 psu during the early summer and 1–3 psu during an extended drought. The observed salinity in 1995 did not reach those higher values, but the model results suggest that the relatively modest increase in channel depth since 1995 associated with the Harbor deepening would increase salinity by 1–1.5 psu for similar drought conditions. While this is modest in absolute terms, it represents an approximate doubling of salinity and a potentially significant impact on the municipal water supply.

The salinity changes extend along the length of the estuary and are not limited to the landward limit of the salinity intrusion. For example, during neap-tide, low-discharge conditions (20 August 1995, $Q_r = 80$ m^3/s), the salinity intrusion extended 95–100 km landward from the Battery, and the lower estuary (<60 km) was strongly stratified in both shipboard survey data (Bowen & Geyer, 2003) and model results using the 1995 bathymetry (Figure 7). In the model with predredging bathymetry, the salinity intrusion extends only 70 km, and the lower estuary has lower salinity and less stratification. During a subsequent spring tide (29 August, $Q_r = 60$ m^3/s), the salinity intrusion had expanded landward to 110 km (as seen in Figure 6) due to the decrease in river discharge, and the stratification was weaker throughout the estuary due to the

Figure 8. Mean salinity and estuarine circulation for constant discharge of 600 m³/s, using (a, b) the predredging (1860) bathymetry and (c, d) the modern (2015) bathymetry.
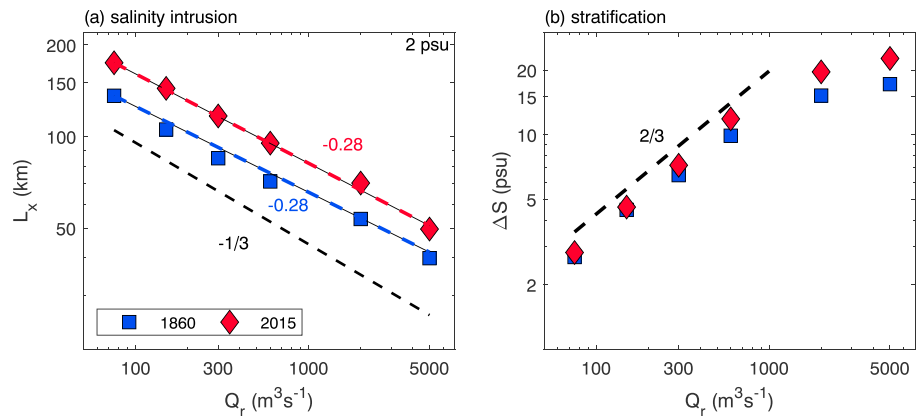
spring tide mixing. The model with the 1995 bathymetry corresponds well with the observations, except for the deep region of the Hudson Highlands (70–80 km) region where the model is more stratified and may be underresolving mixing by small-scale shear and steep side walls. The model with the 1860 bathymetry presents completely different conditions, with the salinity intrusion 30–40 km farther seaward. The stratification in the lower estuary is similar to the 1995 case, which is consistent with the Harbor Water Quality data where differences in stratification were greatest during neap tides (Figure 5).

3.3. Model With Idealized Forcing

To more directly investigate the dependence of the salinity intrusion, stratification, and estuarine circulation on bathymetric changes we use model simulations with idealized forcing, reducing the variability from unsteadiness in the forcing and estuarine response in realistic simulations. The idealized cases span conditions from summer low flow ($Q_r = 75$ m³/s) to a major discharge event (5,000 m³/s). The tidal forcing is simplified but includes M_2, S_2, and N_2 constituents to retain spring-neap variability that is a major factor in the estuary (e.g., Figure 7). To represent average conditions, results in the following analyses are averaged over about 30 days to span multiple spring-neap cycles. For example, $Q_r = 600$ m³/s, which is similar to the average inflow including the Mohawk, Upper Hudson, and smaller tributaries (~550 m³/s), has a salinity intrusion that on average extends 65 km from the Battery with the 2015 bathymetry (Figure 8). For the same discharge, the salinity intrusion decreases to 45 km with predredging bathymetry. In both cases, the estuarine circulation, or vertical structure of the tidally averaged velocity, is landward in the lower layer and seaward in the upper layer in the salinity intrusion, consistent with theory. The estuarine circulation varies along the estuary, but overall the magnitude and spatial patterns of the residual velocity are similar in the two cases.

3.3.1. Salinity Intrusion and Mean Stratification

The increase in salinity intrusion with increased channel depth occurs across the range of constant discharge cases (Figure 9). The landward shift in salinity (based on the 2-psu contour, but similarly for other isohalines) is about 40 km farther landward for the lowest discharge case (75 m³/s) and 10 km for the highest discharge (5,000 m³/s). The proportional increase in estuary length was similar across the discharge cases, with a mean of increase of about 30% and a range of 25% and 37%. For both the modern (2015) and predredging
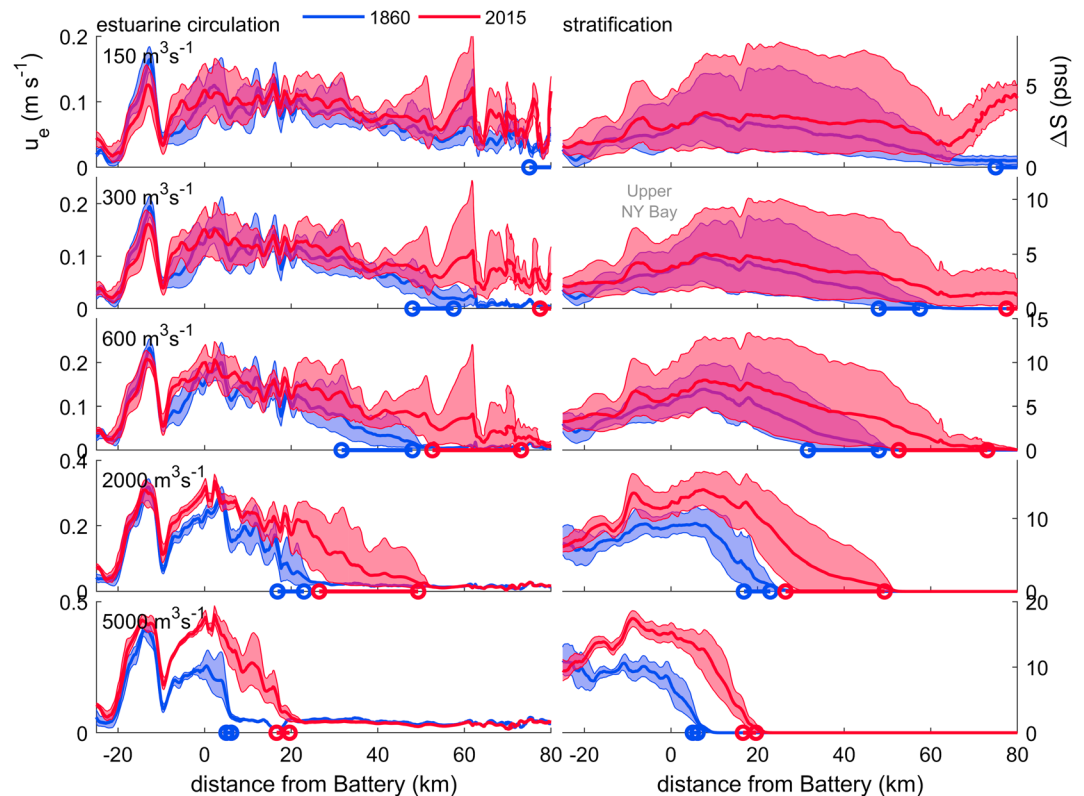
Figure 9. Modeled salinity intrusion and stratification versus discharge. (a) Length of the salinity intrusion (2-psu isohaline) for the predredging and modern bathymetry cases. Best fit regressions are shown along with the $Q_r^{-1/3}$ scaling for steady exchange. (b) Mean stratification (in region with depth-averaged salinity between 10 and 25 psu) for both bathymetry cases, along with a line for the $Q_r^{2/3}$ scaling.

(1860) bathymetries, the best fit dependence of the salinity intrusion on discharge is $Q_r^{-0.28}$. This variability is similar to the analytical solution of $Q_r^{-1/3}$ for a salinity balance dominated by the steady exchange flow (equation (3); MacCready & Geyer, 2010; Monismith et al., 2002) and is consistent with previous observations and model results (Abood, 1974; Hunkins, 1981; Ralston et al., 2008). Hence, dredging has increased the length of the salinity intrusion but not the sensitivity of estuary length to discharge, suggesting that, historically, the dominant salt flux mechanisms (and thus dependence on Q_r) were similar to those today. The amplitude of the increase in estuary length is similar to the $H^{5/3}$ scaling (equation (3)). In the Harbor and lower Hudson (<50 km from the Battery), mean depths in 1860 and 2015 were 15.1 and 17.3 m, respectively, which results in a $H^{5/3}$ scaling factor of 1.3.

Note that to reflect the geomorphic transition to the coastal ocean, the estuary length here is defined by the distance from the mouth of Lower New York Bay, rather than the Battery, which is 25 km farther landward. Some of the most substantial bathymetric changes have occurred seaward of the Battery, in particular the navigational channels through the shoals at the mouth and in the Harbor (Figures 1 and 2). For moderate- to high-discharge conditions, much of the estuarine salinity gradient is located in this part of the estuary, and the changes in bathymetry there affect the entire salinity distribution (Figure 9). Previous studies referencing the salinity intrusion length to the Battery noted an increase in the slope of the power law for L_x versus Q_r for high-discharge conditions (5,000 m^3/s; Abood, 1974). The model results here show that the estuarine response (or slope of L_x versus Q_r) is consistent across the full range of discharge if the estuary length is instead defined relative to the natural mouth.

Mean stratification in the idealized scenarios increases with discharge, and over most of the discharge range the increase in both the 1860 and 2015 bathymetry cases is consistent with the $Q_r^{2/3}$ scaling (equation (5); Hansen & Rattray, 1965; MacCready & Geyer, 2010; Figure 9). The mean stratification ($\Delta S = S_{\text{bottom}} - S_{\text{surface}}$) is averaged over the middle of the salinity distribution, defined as the region with depth-mean salinity between 10 and 25 psu. The $Q_r^{2/3}$ scaling falls off for the highest discharge cases (2,000 and 5,000 m^3/s) where the mean stratifications (20 and 23 psu, respectively, for the 2015 bathymetry) are more than half the maximum salinity and the scaling assumptions become invalid. The proportional increases in mean stratification between the 1860 and 2015 bathymetry cases vary between about 5% for the two lowest discharge cases and 30% for the two highest discharges. In the analytical expression based on the local solution for steady exchange flow (equation (2)), stratification depends on H^3 (Hansen & Rattray, 1965; MacCready & Geyer, 2010), whereas incorporating the dependence of the stratification on $\partial S/\partial x$ leads to a scaling for ΔS as H^{-1}. Using the average estuary depths as above for the salinity intrusion, the two scaling approaches suggest either a 50% increase in stratification or a 10% decrease. In these results the mean stratification increases for all discharge cases, but the increase is much less than the local scaling of H^3 would suggest.
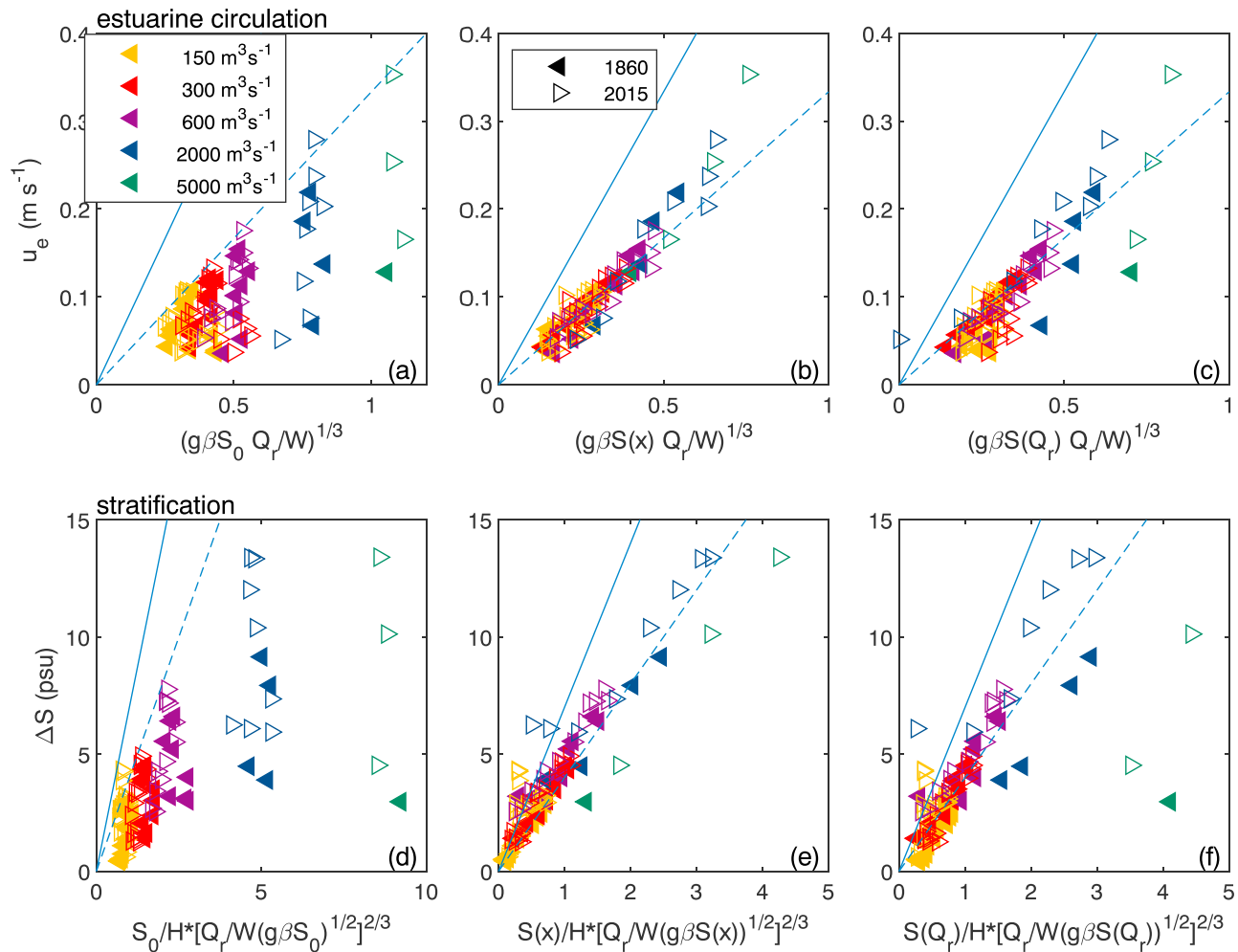
Figure 10. Estuarine circulation and stratification along the estuary. (left) Estuarine circulation versus distance from the Battery for constant discharge from 150 to 5,000 m^3/s for the 1860 and 2015 bathymetry cases. The solid line is mean over 30 days of simulation, and filled surface represents the 15th–85th percentiles. Markers on the *x*-axis show the range of the salinity intrusion for each case (2-psu isohaline, 15th–85th percentiles). (right) Mean stratification along with the 15th–85th percentiles for the same cases. Note the *y*-axis ranges are different for the different discharge cases.

3.3.2. Estuarine Circulation and Stratification

The length of the estuary and mean stratification follow scaling relationships with discharge expected from theory (Figure 9), but these bulk metrics mask significant along-estuary variability (Figure 8) and variability with the spring-neap cycle (Figure 7). For each discharge case, the mean estuarine circulation and typical range (15th–85th percentiles over a 30-day period) is shown as a function of distance along the estuary (Figure 10). Generally, the strength of the estuarine circulation for a given discharge is similar for the pre-dredging and recent bathymetry cases. The results diverge near the landward limit of the salinity intrusion where the estuarine circulation is greater in the 2015 case, but this is because of the greater salinity intrusion (marked as the 15th–85th percentile range of 2-psu isohaline). For both bathymetries the spatial variability in u_e is similar across discharge conditions, for example, with a local minimum at the Narrows and local maxima in the Lower Bay and near the Battery. This suggests that the large-scale variability in the bathymetry due to geologic and geomorphic processes significantly affects the estuarine circulation and that the anthropogenic modifications have not significantly altered those larger-scale patterns.

Stratification also has common along-estuary variability among discharge cases, and the large temporal variability in stratification reflects the importance of the tidal amplitude for vertical mixing (Figure 10). The mean and the maximum stratification with the 2015 bathymetry is greater than with the predredging bathymetry, but particularly for the lower-discharge cases, the spring-neap variability is greater than the average differences due to bathymetry. Bigger increases in stratification are found with the modern bathymetry in the middle and upper parts of the salinity distribution and for the higher-discharge cases. The Upper New York Bay (−10 to 0 km) stands out for increased stratification in the 2015 case, which is consistent with a decrease in mixing due to the large increase in average depth (8.6 to 11.5 m) and decrease in shallow subtidal area (Figure 2). The observational data (Figure 5) also show an overall increase in

Figure 11. Scaling estuarine circulation and stratification for different discharge and bathymetry cases. Marker color represents steady discharge cases from 150 to 5,000 m³/s. Filled markers are the predredging (1860) bathymetry, and open markers are the modern (2015) bathymetry. Estuarine circulation versus scaling from equation (4) (a) using ocean salinity S_0, (b) using local salinity $S(x)$ from the 3-D model, and (c) using local salinity $S(Q_r)$ predicted from Q_r versus L_x. Reference lines have slopes of 2/3 (solid) and 1/3 (dashed). Stratification versus scaling from equation (5) (d) using S_0, (e) using $S(x)$, and (f) using $S(Q_r)$. Reference lines have slopes of 7 (solid) and 4 (dashed).

stratification in the Harbor and lower Hudson, particularly during neap tides, within the natural variability due to forcing conditions.

The estuarine circulation and stratification from the model can be compared with the scaling equations based on the steady exchange theory. To average over shorter-term and smaller-scale variability but resolve spatial gradients along the estuary, the model results are averaged over 30 days and in 5-km segments. We focus here on the Hudson River landward from the Battery because it has a relatively straight, uniform channel and the salt flux is dominated by the exchange flow, consistent with the scaling analysis. Seaward from the Battery, the wider Upper and Lower Bays are separated by the constriction of Verrazano Narrows, and salt flux by tidal process becomes more important and follows different scaling relations, as discussed below.

The scaling based on the local dynamics or the steady state salt balance can be evaluated for how well they predict the along-estuary distribution of estuarine circulation (Figure 11). Using the steady state relationship between $\partial s/\partial x$ and Q_r (equation (4)), the scaling for u_e represents some of the dependence on Q_r, but significant scatter remains within each discharge case due to variation in u_e along the estuary (Figure 11a). That variability largely collapses by using the local mean salinity $S(x)$ rather than S_0 at the ocean boundary in the scaling for u_e (Figure 11b). The scaling in equation (4) was based on a balance between the salt flux

due to the estuarine circulation ($u_e \Delta s$) and the mean advection ($U_0 S_0 = (Q_r/A)S_0$), but the salinity S_0 of the export term applies only at the seaward boundary. As the salinity decreases into the estuary, the seaward advection term decreases in proportion to the salinity (assuming a uniform cross-sectional area), so this local salinity should be used to scale the import by the estuarine circulation.

Using the local salinity from the 3-D model in the scaling is not particularly satisfying, as it is not based on external variables but rather requires a full model simulation. Instead, the local salinity can be estimated based on Q_r by assuming a linear salinity distribution between the mouth and L_x and using equation (3). Using a local salinity based on Q_r in the scaling for u_e (Figure 11c) results in greater scatter than using the salinity from the 3-D model (Figure 11b), but it is a big improvement on using S_0 alone (Figure 11a) and allows prediction of $u_e(x)$ based only on external variables. Using reasonable assumptions for coefficients in equation (4) leads to a slope of about 2/3 (Chant et al., 2018; MacCready & Geyer, 2010), but empirically, the slope in these results is about half that value. The scaling for u_e seems to work similarly well for the pre-dredging and modern bathymetry cases, which is consistent with the independence of u_e with depth in equation (4) and with the similarity in u_e between the two cases (Figure 10).

Stratification in the model can be compared with the scaling in equation (5) to account for some of the range of ΔS with discharge, but significant variability remains spatially and between bathymetry cases (Figure 11d). Using the local salinity $s(x)$ taken from the model reduces this variability considerably, and using an estimate of the local salinity based on Q_r as above provides a similar collapse (Figures 11e and 11f). The slope in equation (5) is about 7 based on coefficients in MacCready and Geyer (2010), but here the slope is about half to two thirds of that.

The scaling results for u_e were similar for the predredging and modern bathymetry cases (Figures 11a–11c), but there is a greater discrepancy between the two bathymetries for ΔS. The stratification in the model with the 2015 bathymetry is generally greater than that for the 1860 bathymetry (Figures 11d–11f). For example, the best fit slope (for $Q_r < 2{,}000$ m^3/s) using local salinity estimated from Q_r (Figure 11f) is 3.4 for the 1860 bathymetry and 4.8 for the 2015 bathymetry, consistent with the greater stratification after channel deepening. While the scaling in equation (5) indicates that ΔS should decrease with the greater channel depth, the observations and model results indicate the opposite, with a slight increase. The differences in best fit slopes between the bathymetry cases suggest that additional factors are missing in the scaling for mean stratification, a topic that is considered in the discussion.

3.3.3. Salt Flux

The conceptual framework for the scaling of u_e and ΔS is based on the assumption that the steady exchange flow dominates the total salt flux, but tidal salt fluxes may have been more important in a shallower, shorter estuary prior to channel deepening. Observations in the lower Hudson (23 km from Battery) in 2002 showed that the steady, residual salt flux was the dominant contributor to the total (Lerczak et al., 2006). The residual flux in that study varied by an order of magnitude—maximal during neap tides when the estuarine circulation and stratification were the greatest and reduced during spring tides when the steady circulation was less than the tidal component. Averaged over several months, the ratio of the tidal diffusive salt flux to the total, or ν (Hansen & Rattray, 1966), was 0.12 (Lerczak et al., 2006). Observations at 10 km under lower-discharge conditions (100–300 m^3/s) in 1995 found that the tidal diffusive salt flux was about 30% of the total ($\nu = 0.3$), consistent with a local enhancement of the tidal component during low discharge (Bowen & Geyer, 2003). Similarly, at the Narrows the steady salt flux increased by about a factor of 5 between low- and high-discharge periods, but even during low flow the steady exchange was about 5 times greater than the tidal contribution (Hunkins, 1981).

The salt flux can be calculated directly in the model and decomposed into tidal residual and tidally varying components. With similar averaging of 30 days and 5-km bins as for u_e and ΔS, the ratio of the tidal diffusive salt flux to the total averages around 0.25 for all the discharge cases, varying between about 0.2 for higher-discharge and 0.3 for lower-discharge cases. With the shallower 1860 bathymetry and shorter tidal intrusion, the tidal salt flux represents a slightly greater fraction of the total, averaging between 0.3 for low discharge and 0.4 for high discharge. In both cases, the results are consistent with the observed dominance of the steady salt flux, but there is significant spatial and temporal variation in ν along the estuary and with forcing conditions. With both the predredging and modern bathymetries, ν varies between 0.1 and 0.4 along the estuary, with similar spatial patterns between the bathymetry cases. Only near the mouth does the tidal

component consistently account for more than half of the total salt flux ($\nu > 0.5$). The model results indicate that the tidal contribution to the salt flux was greater in the predredging estuary, but the steady exchange flow was the dominant factor and the scaling relationships for u_e and ΔS based on that assumption generally hold.

4. Summary and Discussion

Based on evidence from both observations and models, deepening the Hudson River estuary has increased the length of the salinity intrusion and moderately increased the stratification. The expansion of the salinity intrusion landward is largely consistent with the scaling of $H^{5/3}$ for an estuary dominated by steady salt flux. The increase in estuary length has not affected its sensitivity to river discharge, with approximately a $Q_r^{-1/3}$ dependence in both the predredging and modern model results. The mean stratification has increased, particularly during neap tides, but again the dependence on discharge is similar in the predredging and modern cases and is consistent with theory that ΔS scales with $Q_r^{2/3}$. A comparison of the salt flux mechanisms finds that while the steady salt flux is a slightly greater fraction of the total in the modern Hudson than in the shallower, shorter estuary before dredging, the tidal salt flux contributes less than half the total in both cases. Tidal amplitudes in the lower estuary have increased moderately with channel deepening (Ralston et al., 2019), and while this might be expected to increase the tidal salt flux, the increases in steady salt flux have been even greater. Increased tidal velocities would be expected to reduce the length of the salinity intrusion based on the steady salt flux scaling (equation (3)), but in the saline part of the Hudson (<120 km from the Battery), the increases in tidal amplitude have been relatively modest (10–40%) compared with those farther landward in the fresh tidal river (>100%; Ralston et al., 2019). According to model results, tidal velocities have increased by up to 30% in some regions of the saline estuary, but increase on average is only 10%. Effects of increased tidal velocity on reducing the salinity intrusion are more than offset by the effects of the increase in depth.

Somewhat paradoxically, channel deepening in the Hudson appears not to have significantly increased the estuarine circulation. While the local scaling suggests a dependence on H^2, or a 34% increase using the average depth increase, the increase in salinity intrusion and decrease in salinity gradient results in a steady state scaling for u_e that is independent of depth (Chant et al., 2018). In contrast, analysis of observations from Kill van Kull found that the estuarine circulation increased with deepening (Chant et al., 2018). In Kill van Kull, the salinity gradient is constrained by the geometry, unlike in the Hudson where it can freely adjust to changes in the forcing. The results here show that the estuarine circulation along the Hudson can be scaled based on equation (4) but that it is important to use the local salinity rather than S_0 at the ocean boundary. The relatively robust relationship between L_x and $Q_r^{-1/3}$ allows reasonable prediction of the local salinity based only on external variables rather than requiring 3-D model results. Note that these results all are based on monthly averages, and do not incorporate the variability in L_x and u_e at spring-neap time scales that can be substantial (Ralston et al., 2008).

Scaling from Chant et al. (2018) showed that the stratification should decrease with channel deepening and landward expansion of the salinity intrusion, but in the Hudson observations and model results indicate that the stratification has instead increased, particularly during neap tides. The increase in stratification suggests a decrease in mixing. Full water-column mixing that is implicit in the scaling of K_S with thalweg depth (equations (2) and (5)) rarely occurs in the Hudson, as stratification in the deeper parts of channel limits the height of the bottom boundary layer to less than the full depth. In model results using the modern bathymetry, much of the mixing occurs on lateral shoals rather than in the deep channel, particularly where salinity fronts form at constrictions during ebbs (Geyer & Ralston, 2015). The fronts extend laterally onto the shoals where bottom boundary layer turbulence interacts with the frontal salinity gradients to account for more than half of the total mixing in the estuary. The analyses here have focused on the increases in channel thalweg depth, but there have also been significant decreases in shallow subtidal area due to infilling and narrowing of channels (Figure 2). The loss of shallow subtidal would reduce the area where salinity gradients might otherwise intersect with the bottom boundary layer and mix, and could contribute to the overall increase in stratification. The response of stratification in the Hudson to channel deepening does not reflect the predictions of either equation (2) or (5), indicating that a revised theoretical framework is needed to incorporate missing factors or processes.

The increase in channel depth corresponds with a shift in estuarine parameter space (Geyer & MacCready, 2014). One key parameter is the freshwater Froude number $Fr_f = U_0/(\beta g S_0 H)^{1/2}$, which represents the ratio of the mean river velocity (U_0) and the gravitationally driven exchange flow that is scaled based on the depth H and ocean salinity S_0. Another is the mixing parameter $M = \left[C_d U_t^2/\omega N_0 H^2\right]^{1/2}$, which compares the vertical mixing time scale to the tidal frequency ω for the maximum buoyancy frequency $N_0 = (\beta g S_0/H)^{1/2}$, tidal velocity U_t, and drag coefficient C_d. The two parameters can be used to characterize differences between estuaries in characteristics such as stratification and estuary length across a range of bathymetric configurations and forcing conditions (Geyer & MacCready, 2014). In this parameter space, the modern Hudson falls between strongly stratified and partially mixed regions, with temporal variation in Fr_f and M depending on river discharge and tidal amplitude. The dependence of Fr_f on $H^{-1/2}$ and of M on $H^{-3/4}$ (assuming depth changes do not significantly affect U_t or U_0) results in proportional decreases of these parameters of about 7% and 10%, respectively, based on the average increase in thalweg depth in the lower estuary. The decreases in both these parameters shift the Hudson toward the "strongly stratified" part of parameter space, but the changes in their mean values are small compared to the variability with tidal and river forcing. Seasonal variation between spring freshet and summer low discharge corresponds with an order of magnitude variation in Fr_f, and spring-neap tidal amplitude changes M by about a factor of 2. The modest shifts in estuarine parameter space due to dredging (or the relative insensitivity of the parameters to depth) compared with the time dependence of the forcing are consistent with the modest effects on the stratification and salt flux mechanisms.

While dredging has not significantly altered the dominant means of estuarine exchange in the Hudson, it has significantly increased the landward extent of the salinity intrusion (Figure 9). During low flow, the salinity intrusion now reaches 110 km or more, which puts at risk the public drinking water supply withdrawn from the Hudson by Poughkeepsie (NY; Bowen & Geyer, 2003). A regulatory framework maintains discharge from the Upper Hudson through reservoir releases so that the salinity intrusion remains seaward of this water intake, but the associated economic costs due to lost hydropower generation capacity can be significant during extended drought periods. During droughts in the summers of 1985 and 1995 the salinity intrusion threatened the water supply, but reports of similar problems back to 1913 (Fowell, 1913) are consistent with the model findings here that the creation of Ambrose Channel may have increased the salinity intrusion more than 100 km upstream. Seaward from Poughkeepsie, emergency water intakes for the New York City water supply are located ~90 km from the Battery. During the 1985 drought more than 100 million gallons per day of salty water were extracted from the Hudson, requiring dilution with fresher sources prior to distribution (Greer, 1985). Extended drought conditions limit water supply sources regionally and increase municipal consumption, increasing the role of the emergency pumps during the periods when the salinity intrusion is most likely to extend past the intakes. Tree ring reconstructions suggest that the past several decades are among the wettest in the Hudson watershed over the past 500 years, so a return to more typical hydrological conditions would only exacerbate the threats to water supplies (Pederson et al., 2013).

Another human impact of salt-water intrusion is on commercial shellfish resources. The lower Hudson and New York Harbor once supported an abundant, commercially important oyster population, but overfishing, habitat loss, and pollution led to severe declines by the early twentieth century (Franz, 1982). Oyster restoration efforts in the Hudson have intensified in recent years, but the success of constructed oyster reefs depends on both suitable substrate (hard bottom, shallow depth) and optimal salinity for growth and disease resistance (Levinton et al., 2011; Starke et al., 2011). Historically, some of the richest oyster beds were in shallow regions of the Upper Bay (Franz, 1982). Water quality has improved substantially since the period of oyster population decline, but infilling of shallow subtidal and salinity increases in the lower estuary both tend to reduce the suitable habitat for restoration. Channel deepening has increased the landward extent of the salinity intrusion and potentially created new regions of suitable habit farther up-estuary, but bedrock constraints make much of the Hudson narrow, limiting the suitable substrate within the optimal salinity range (Starke et al., 2011).

Channel modifications and the resulting changes in hydrodynamic conditions also have the potential to alter sediment transport in the estuary. Several European estuaries, including the Ems and the Loire, have had increases in both tidal amplitude and suspended sediment associated with dredging (de Jonge et al.,

2014; Jalón-Rojas et al., 2016; Talke et al., 2009). A positive feedback between tidal amplification, sediment resuspension, and reduction of drag by fluid mud is thought to cause the rapid accumulation of sediment and a potential regime shift to a hyperturbid state (Winterwerp et al., 2013). In that conceptual model sediment trapping is driven primarily by tidal asymmetry, but sediment trapping by the residual circulation could also be enhanced by deepening (Burchard et al., 2018). Tidal amplitude has more than doubled due to dredging in the tidal freshwater region of the upper ~60 km of the Hudson, but the increases in tidal amplitude in the harbor and lower estuary have been smaller (Ralston et al., 2019), so the corresponding effects on sediment transport are expected to be small. The increase in salinity intrusion is likely to increase the landward extent of sediment trapping, change the location of estuarine turbidity maxima, and increase the time scales for transport through the estuary (Ralston & Geyer, 2018). However, to this point the Hudson has not undergone a dramatic shift in sediment concentration like that observed in several European estuaries.

References

Abood, K. A. (1974). Circulation in the Hudson estuary. *Annals of the New York Academy of Sciences*, *250*(1 Hudson River), 39–111. https://doi.org/10.1111/j.1749-6632.1974.tb43895.x

Amin, M. (1983). On perturbations of harmonic constants in the Thames Estuary. *Geophysical Journal International*, *73*(3), 587–603. https://doi.org/10.1111/j.1365-246X.1983.tb03334.x

Andrews, S. W., Gross, E. S., & Hutton, P. H. (2017). Modeling salt intrusion in the San Francisco Estuary prior to anthropogenic influence. *Continental Shelf Research*, *146*, 58–81. https://doi.org/10.1016/j.csr.2017.07.010

Bowen, M. M., & Geyer, W. R. (2003). Salt transport and the time-dependent salt balance of a partially stratified estuary. *Journal of Geophysical Research*, *108*(C5), 3158. https://doi.org/10.1029/2001JC001231

Burchard, H., Schuttelaars, H. M., & Ralston, D. K. (2018). Sediment trapping in estuaries. *Annual Review of Marine Science*, *10*(1), 371–395. https://doi.org/10.1146/annurev-marine-010816-060535

Chant, R. J., Sommerfield, C. K., & Talke, S. A. (2018). Impact of channel deepening on tidal and gravitational circulation in a highly engineered estuarine basin. *Estuaries and Coasts*, *41*(6), 1587–1600. https://doi.org/10.1007/s12237-018-0379-6

de Jonge, V. N., Schuttelaars, H. M., van Beusekom, J. E. E., Talke, S. A., & de Swart, H. E. (2014). The influence of channel deepening on estuarine turbidity levels and dynamics, as exemplified by the Ems estuary. *Estuarine, Coastal and Shelf Science*, *139*, 46–59. https://doi.org/10.1016/j.ecss.2013.12.030

DiLorenzo, J. L., Huang, P., Llewellyn Thatcher, M., & Najarian, T. O. (1993). Dredging impacts on Delaware estuary tides. In *Proceedings of the 3rd International Conference on Estuarine and Coastal Modeling III* (pp. 86–104).

Familkhalili, R., & Talke, S. A. (2016). The effect of channel deepening on tides and storm surge: A case study of Wilmington, NC. *Geophysical Research Letters*, *43*, 9138–9147. https://doi.org/10.1002/2016GL069494

Fowell, A. P. (1913). Ashokan Reservoir increases salinity of Hudson. In *Municipal Journal*, December 4 (23rd ed., Vol. 35, p. 771). New York: Municipal Journal and Engineer, Inc.

Franz, D. R. (1982). An historical perspective on mollusks in lLower New York hHarbor, with emphasis on oysters. In *Ecological Stress and the New York Bight: Science and Management* (pp. 181–197). Columbia SC: Estuarine Research Federation.

Geyer, W. R., & MacCready, P. (2014). The estuarine circulation. *Annual Review of Fluid Mechanics*, *46*(1), 175–197. https://doi.org/10.1146/annurev-fluid-010313-141302

Geyer, W. R., & Ralston, D. K. (2015). Estuarine frontogenesis. *Journal of Physical Oceanography*, *45*(2), 546–561. https://doi.org/10.1175/JPO-D-14-0082.1

Greer, W. R. (1985). Salt in Hudson imperils Poughkeepsie water. *New York Times*, August 25.

Haidvogel, D. B., Arango, H., Budgell, W. P., Cornuelle, B. D., Curchitser, E., Di Lorenzo, E., et al. (2008). Ocean forecasting in terrain-following coordinates: Formulation and skill assessment of the Regional Ocean Modeling System. *Journal of Computational Physics*, *227*(7), 3595–3624. https://doi.org/10.1016/j.jcp.2007.06.016

Hansen, D. V., & Rattray, M. (1965). Gravitational circulation in straits and estuaries. *Journal of Marine Research*, *23*, 104–122.

Hansen, D. V., & Rattray, M. (1966). New dimensions in estuary classification. *Limnology and Oceanography*, *11*(3), 319–326. https://doi.org/10.4319/lo.1966.11.3.0319

Hunkins, K. (1981). Salt dispersion in the Hudson estuary. *Journal of Physical Oceanography*, *11*(5), 729–738. https://doi.org/10.1175/1520-0485(1981)011<0729:SDITHE>2.0.CO;2

Hutton, P. H., Rath, J. S., Chen, L., Ungs, M. J., & Roy, S. B. (2015). Nine decades of salinity observations in the San Francisco Bay and Delta: Modeling and trend evaluations. *Journal of Water Resources Planning and Management*, *142*(3), 04015069. https://doi.org/10.1061/(ASCE)WR.1943-5452.0000617

Jalón-Rojas, I., Sottolichio, A., Hanquiez, V., Fort, A., & Schmidt, S. (2018). To what extent multidecadal changes in morphology and fluvial discharge impact tide in a convergent (turbid) tidal eiver. *Journal of Geophysical Research: Oceans*, *123*(5), 3241–3258. https://doi.org/10.1002/2017JC013466

Jalón-Rojas, I., Schmidt, S., Sottolichio, A., & Bertier, C. (2016). Tracking the turbidity maximum zone in the Loire Estuary (France) based on a long-term, high-resolution and high-frequency monitoring network. *Continental Shelf Research*, *117*, 1–11. https://doi.org/10.1016/j.csr.2016.01.017

Jay, D. A., Leffler, K., & Degens, S. (2011). Long-term evolution of Columbia River tides. *Journal of Waterway, Port, Coastal, and Ocean Engineering*, *137*(4), 182–191. https://doi.org/10.1061/(ASCE)WW.1943-5460.0000082

Klingbeil, A. D., & Sommerfield, C. K. (2005). Latest Holocene evolution and human disturbance of a channel segment in the Hudson River estuary. *Marine Geology*, *218*(1-4), 135–153. https://doi.org/10.1016/j.margeo.2005.02.026

Lerczak, J. A., Geyer, W. R., & Chant, R. J. (2006). Mechanisms driving the time-dependent salt flux in a partially stratified estuary. *Journal of Physical Oceanography*, *36*(12), 2296–2311. https://doi.org/10.1175/JPO2959.1

Levinton, J., Doall, M., Ralston, D., Starke, A., & Allam, B. (2011). Climate change, precipitation and impacts on an estuarine refuge from disease. *PLOS ONE*, *6*(4), e18849. https://doi.org/10.1371/journal.pone.0018849

MacCready, P. (1999). Estuarine adjustment to changes in river flow and tidal mixing. *Journal of Physical Oceanography*, *29*(4), 708–726. https://doi.org/10.1175/1520-0485(1999)029<0708:EATCIR>2.0.CO;2

MacCready, P., & Geyer, W. R. (2010). Advances in estuarine physics. *Annual Review of Marine Science*, *2*(1), 35–58. https://doi.org/10.1146/annurev-marine-120308-081015

Meyers, S. D., Linville, A. J., & Luther, M. E. (2014). Alteration of residual circulation due to large-scale infrastructure in a coastal plain estuary. *Estuaries and Coasts*, *37*(2), 493–507. https://doi.org/10.1007/s12237-013-9691-3

Mitchell, H. (1887). Report on the results of the physical surveys of New York Harbor. Appendix No. 1887-15. *Coast and Geodetic Survey Annual Reports.*, 301–311. ftp://ftp.library.noaa.gov/docs.lib/htdocs/rescue/cgs/002_pdf/CSC-0086.PDF

Monismith, S. G., Kimmerer, W., Burau, J. R., & Stacey, M. T. (2002). Structure and flow-induced variability of the subtidal salinity field in northern San Francisco Bay. *Journal of Physical Oceanography*, *32*(11), 3003–3019. https://doi.org/10.1175/1520-0485(2002)032<3003:SAFIVO>2.0.CO;2

Mukai, A. Y., Westerink, J. J., Luettich, R. A. Jr., & Mark, D. (2002). Eastcoast 2001, a tidal constituent database for western North Atlantic, Gulf of Mexico, and Caribbean Sea. DTIC Document.

New York City Department of Environmental Protection (2010). *New York Harbor Survey Program celebrating 100 years*. Flushing, NY, New York City Department of Environmental Protection.

New York Metropolitan Sewerage Commission (1909). *Digest of data collected before the year 1908, relating to the sanitary condition of New York harbor*. New York: M.B. Brown Press.

Pederson, N., Bell, A. R., Cook, E. R., Lall, U., Devineni, N., Seager, R., et al. (2013). Is an epic pluvial masking the water insecurity of the greater New York City region. *Journal of Climate*, *26*(4), 1339–1354. https://doi.org/10.1175/JCLI-D-11-00723.1

Ralston, D. K., & Geyer, W. R. (2018). Sediment transport time scales and trapping efficiency in a tidal river. *Journal of Geophysical Research: Earth Surface*, *122*(11), 2042–2063. https://doi.org/10.1002/2017JF004337

Ralston, D. K., Geyer, W. R., & Lerczak, J. A. (2008). Subtidal salinity and velocity in the Hudson River estuary: Observations and modeling. *Journal of Physical Oceanography*, *38*(4), 753–770. https://doi.org/10.1175/2007JPO3808.1

Ralston, D. K., Talke, S., Geyer, W. R., Al-Zubaidi, H. A. M., & Sommerfield, C. K. (2019). Bigger tides, less flooding: Effects of dredging on barotropic dynamics in a highly modified estuary. *Journal of Geophysical Research: Oceans*, *124*(1), 196–211. https://doi.org/10.1029/2018JC014313

Starke, A., Levinton, J. S., & Doall, M. (2011). Restoration of *Crassostrea virginica* (Gmelin) to the Hudson River, USA: A spatiotemporal modeling approach. *Journal of Shellfish Research*, *30*(3), 671–684. https://doi.org/10.2983/035.030.0309

Talke, S. A., de Swart, H. E., & Schuttelaars, H. M. (2009). Feedback between residual circulations and sediment distribution in highly turbid estuaries: An analytical model. *Continental Shelf Research*, *29*(1), 119–135. https://doi.org/10.1016/j.csr.2007.09.002

Talke, S. A., Orton, P., & Jay, D. A. (2014). Increasing storm tides in New York Harbor, 1844–2013. *Geophysical Research Letters*, *41*, 3149–3155. https://doi.org/10.1002/2014GL059574

Wall, G., Nystrom, E., & Litten, S. (2008). Suspended sediment transport in the freshwater reach of the Hudson River estuary in eastern New York. *Estuaries and Coasts*, *31*(3), 542–553. https://doi.org/10.1007/s12237-008-9050-y

Warner, J. C., Armstrong, B., He, R., & Zambon, J. B. (2010). Development of a Coupled Ocean–Atmosphere–Wave–Sediment Transport (COAWST) Modeling System. *Ocean Modelling*, *35*(3), 230–244. https://doi.org/10.1016/j.ocemod.2010.07.010

Winterwerp, J. C., Wang, Z. B., van Braeckel, A., van Holland, G., & Kösters, F. (2013). Man-induced regime shifts in small estuaries—II: A comparison of rivers. *Ocean Dynamics*, *63*(11-12), 1293–1306. https://doi.org/10.1007/s10236-013-0663-8

Zhang, E., Savenije, H. H. G., Wu, H., Kong, Y., & Zhu, J. (2011). Analytical solution for salt intrusion in the Yangtze Estuary, China. *Estuarine, Coastal and Shelf Science*, *91*(4), 492–501. https://doi.org/10.1016/j.ecss.2010.11.008

Zhu, J., Weisberg, R. H., Zheng, L., & Han, S. (2015). Influences of channel deepening and widening on the tidal and nontidal circulations of Tampa Bay. *Estuaries and Coasts*, *38*(1), 132–150. https://doi.org/10.1007/s12237-014-9815-4